Supporting Information

Boosting Oxygen Evolution Reaction by Bulk-Confined Zn Doping in NiFe-LDH Anchored on Stainless Steel Foam

Yuxin Liu [a], Yandi Wen [b, c], Xiangjie Liu [b], Guodong Xu [d], Changyuan Bao [d], Xiao Yang [a], Lingfeng Li [b, c, *]

[a] College of Chemical and Environmental Engineering, Yancheng Teachers University, Yancheng 224051, China
[b] Advanced Battery Technology Center, School of Marine Science and Technology, Harbin Institute of Technology, Weihai 264209, China
[c] Harbin Institute of Technology (Weihai) Qingdao Research Institute Qingdao 266109, China
[d] School of Green and Low-carbon, Yancheng Teachers University, Yancheng 224051, China

* Corresponding author: Lingfeng Li (lilingfeng@hit.edu.cn).

Experimental Section

Chemicals and Reagents

Iron nitrate nonahydrate ($Fe(NO_3)_3·9H_2O$), nickel nitrate hexahydrate ($Ni(NO_3)_2·6H_2O$), zinc nitrate hexahydrate ($Zn(NO_3)_2·6H_2O$), potassium hydroxide (KOH), and hydrochloric acid (HCl) were purchased from Aladdin. Stainless steel foam (316 L) was purchased from *taobao*. All regents was used without any further purification.

Synthesis of hierarchical Zn@NiFe-LDH/SSF

The hierarchical structured catalyst, denoted as Zn@NiFe-LDH, was synthesized through a sequential two-step electrodeposition protocol. Prior to deposition, a stainless steel foam (SSF, 1.0 × 0.5 cm^2) substrate was ultrasonically cleaned sequentially in ethanol, 1 M HCl, deionized water, and ethanol again. In the first step, the pre-cleaned SSF (working electrode) and a Pt foil (counter electrode) were immersed in an aqueous solution containing $Ni(NO_3)_2·6H_2O$ (30 mM), $Fe(NO_3)_3·9H_2O$ (10 mM), and $Zn(NO_3)_2·6H_2O$ (2 mM). A constant potential of -1.0 V (vs. SCE) was applied for 5 minutes. Subsequently, the sample was rinsed and subjected to a second step of electrodeposition for another 5 minutes in a fresh solution containing only $Ni(NO_3)_2·6H_2O$ (30 mM) and $Fe(NO_3)_3·9H_2O$ (10 mM), under identical potential conditions. For the controlled variation of Zn electrodeposition amount, electrodeposition was first carried out in a Zn-containing electrolyte for x minutes. Subsequently, the sample was rinsed and subjected to a second step of electrodeposition for (10-x) minutes in a fresh solution containing only $Ni(NO_3)_2·6H_2O$ (30 mM) and $Fe(NO_3)_3·9H_2O$ (10 mM), under identical potential conditions. The notation ‘x’ in the sample name represents the duration (in minutes) of the first electrodeposition step in the Zn-containing electrolyte. For the sake of simplicity and clarity in manuscript, Zn_5@NiFe-LDH and Zn_{10}@NiFe-LDH are abbreviated as Zn@NiFe-LDH and Zn-NiFe-LDH.

Synthesis of Conventional Zn-NiFe-LDH and NiFe-LDH on SSF

For comparison, the conventional Zn-doped NiFe-LDH (Zn-NiFe-LDH) catalyst was prepared using a one-step electrodeposition method identical to the first step of the Zn@NiFe-LDH/SSF synthesis for a total duration of 10 minutes. The pristine NiFe-LDH

catalyst was prepared via the same one-step electrodeposition method (10 minutes) in a Zn-free solution containing $Ni(NO_3)_2 \cdot 6H_2O$ (30 mM) and $Fe(NO_3)_3 \cdot 9H_2O$ (10 mM).

Characterization

The phase structure of the samples was determined via X-ray diffraction (XRD, Bruker D8 advance, Cu Kα radiation) with a scan rate of 10° min^{-1}. The material's morphologies were assessed through sfield emission scanning electron microscope (SEM, Quanta 200 FEG) and transmission electron microscopy (TEM, Hitachi-2100, 200 kV), coupled with energy-dispersive X-ray spectrometry (EDS) for elemental mapping. X-ray photoelectron spectroscopy (XPS, Thermo Scientific K-Alpha) analyse was used to analyze the surface chemical composition. Additionally, Raman spectra were acquired by utilizing Evolution Horiba Scientific-LabRAM HR system.

Electrochemical Measurements

All electrochemical measurements were performed using a CHI 660e electrochemical workstation (Shanghai Chenhua) with a standard three-electrode configuration in 1.0 M KOH electrolyte at room temperature. A graphite rod and a Hg/HgO (1.0 M KOH) electrode were used as the counter electrode and reference electrode, respectively. The working electrode was prepared by depositing the catalyst on stainless steel foam (SSF).

Cyclic voltammetry (CV) was conducted at a scan rate of 100 mV s^{-1}. Linear sweep voltammetry (LSV) was carried out in the same potential window at a sweep rate of 10 mV s^{-1} to obtain OER polarization curves. Electrochemical impedance spectroscopy (EIS) measurements were performed at 1.23 V (vs. RHE) with an AC amplitude of 5 mV over a frequency range of 100 kHz to 0.1 Hz.

All measured potentials were referenced to the reversible hydrogen electrode (RHE) using the conversion equation: $E_{RHE}=E_{Hg/HgO}+0.059\times pH+0.098$ V. Additionally, 90% *iR* compensation was applied to all polarization curves based on the solution resistance. The long-term stability of the catalysts was evaluated by chronoamperometry at a constant overpotential corresponding to an initial overpotential of 500 mV for 100 hours.

Theoretical calculation

All density functional theory (DFT) calculations were carried out using the Vienna *ab*

initio Simulation Package (VASP). The electron exchange-correlation interactions were described within the generalized gradient approximation (GGA) using the Perdew-Burke-Ernzerhof (PBE) functional. The plane-wave basis set was expanded with a cutoff energy of 450 eV. Geometric structures were optimized until the total energy and atomic forces converged to below 1×10^{-5} eV and 0.03 eV/Å, respectively. The Brillouin zone was sampled with a Gamma-centered 2 × 2 × 1 k-point grid generated by the Monkhorst-Pack method. The oxygen evolution reaction (OER) mechanism was investigated based on a four-electron lattice oxygen-mediated mechanism (LOM) pathway. The Gibbs free energies of reaction intermediates were calculated using the computational hydrogen electrode (CHE) model developed by Nørskov and coworkers. The NiFe-layered double hydroxide (LDH) catalyst was modeled using a periodic slab with two atomic layers, all of which were allowed to relax during optimization. The free energy corrections, including zero-point energy and entropy contributions, were applied to the adsorbed intermediates.

Supplementary Figures and Tables

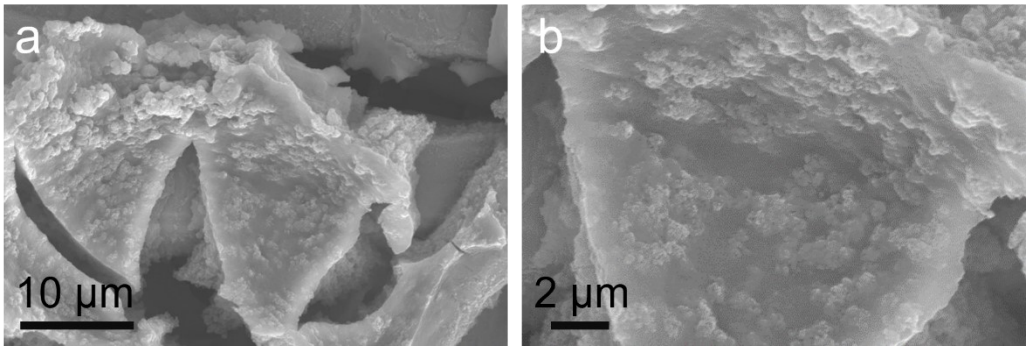

Fig. S1 SEM images of NiFe-LDH.

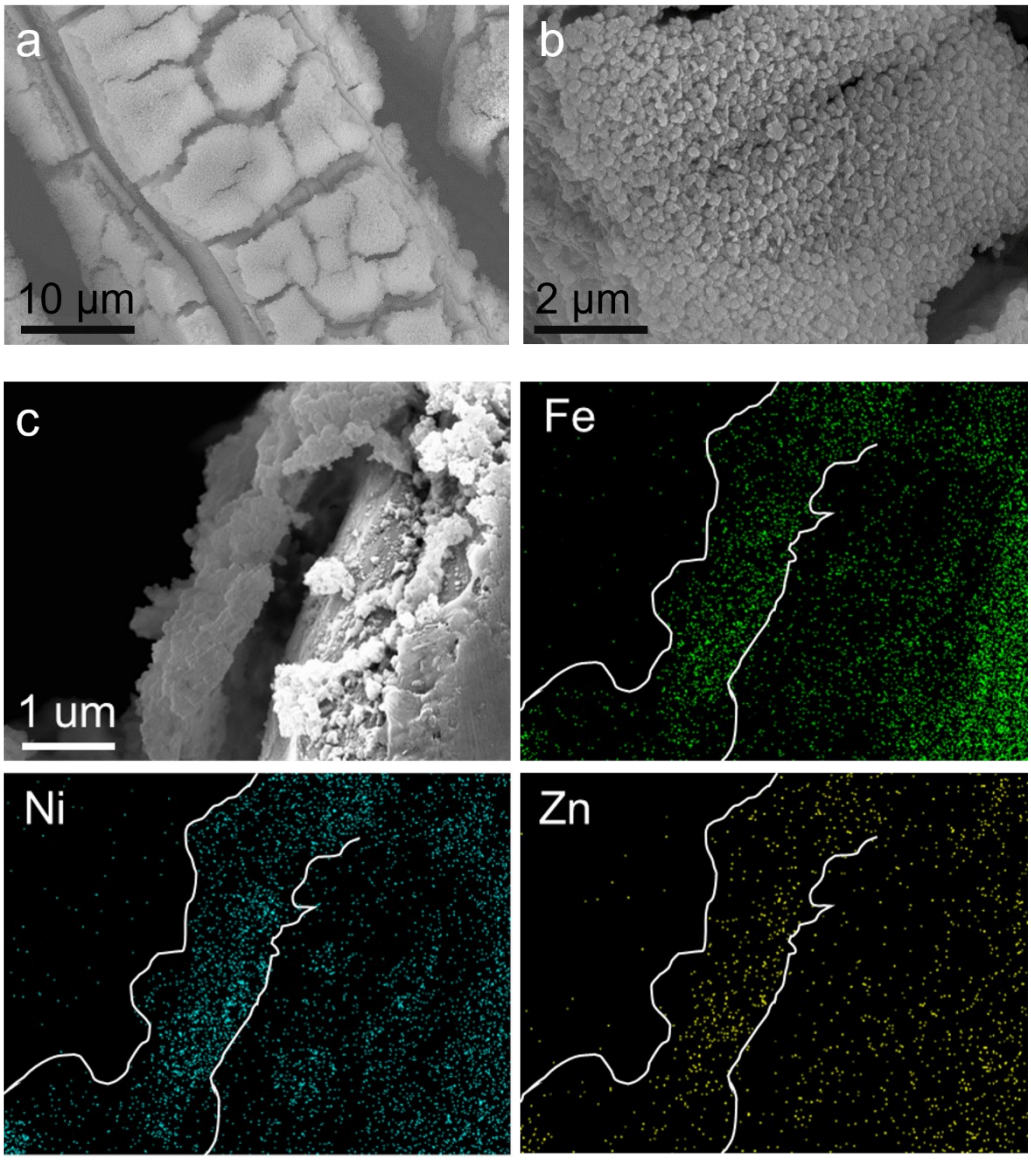

Fig. S2 SEM images (a, b, c) and the corresponding elemental mapping (d) of Ni, Fe, and Zn for Zn@NiFe-LDH.

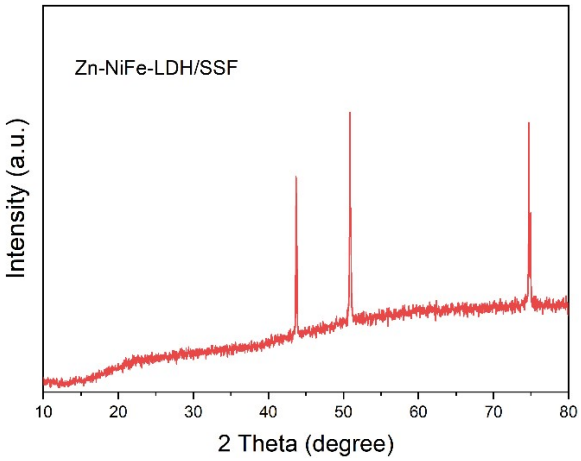

Fig. S3 XRD patterns of Zn-NiFe-LDH.

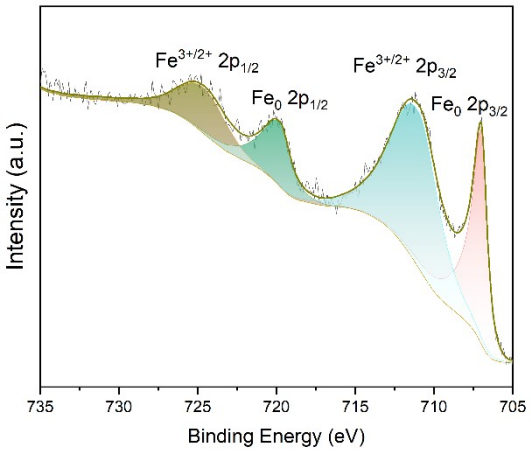

Fig. S4 High-resolution Fe 2p spectra of SSF.

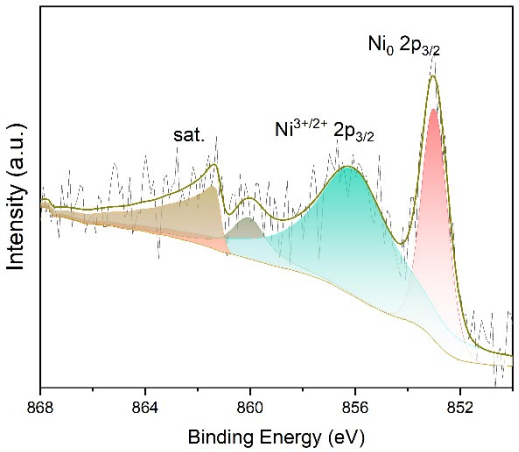

Fig. S5 High-resolution Ni 2p spectra of SSF.

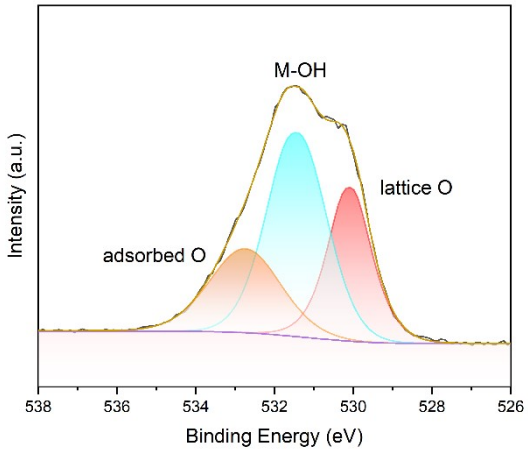

Fig. S6 High-resolution O 1s spectra of SSF.

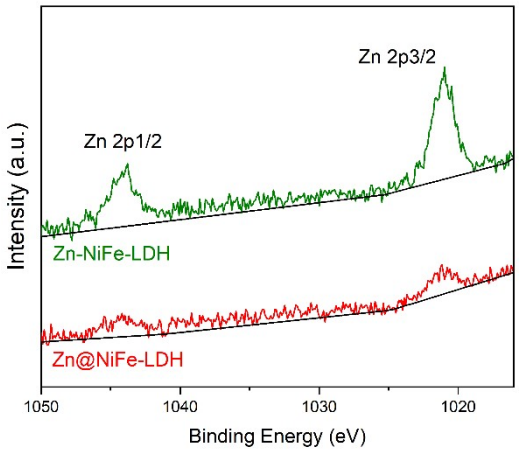

Fig. S7 High-resolution Zn 2p spectra of Zn-NiFe-LDH and Zn@NiFe-LDH.

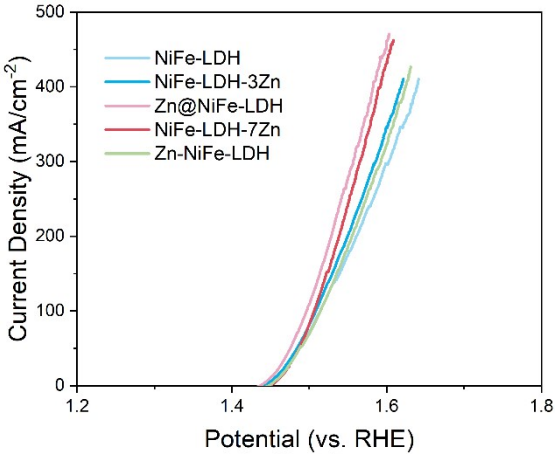

Fig. S8 LSV curves of Zn_x@NiFe-LDH in 1.0 M KOH .

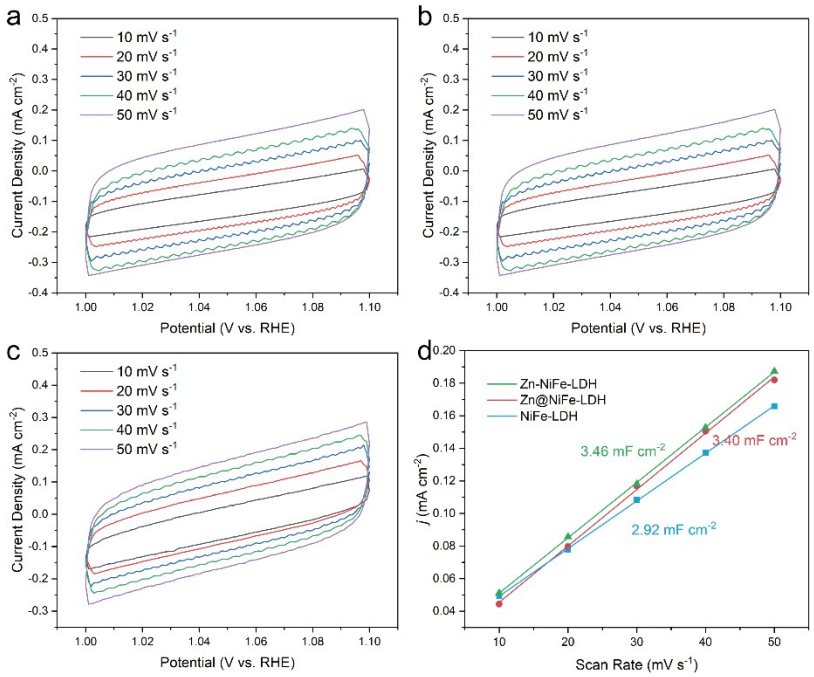

Fig. S9 CV curves at different scan rates from 10 to 20 mV s^{-1} for NiFe-LDH (a), Zn@NiFe-LDH (b), Zn-NiFe-LDH (c) in 1 M KOH. (d) the corresponding C_{dl} plots.

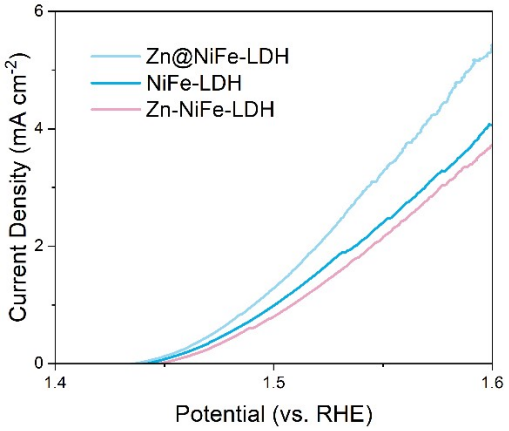

Fig. S10 ECSA-normalized LSV curves of Zn@NiFe-LDH and other control samples.

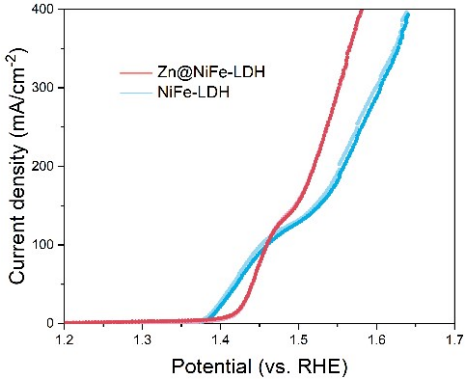

Fig. S11 Initial and post-stability LSV curves of Zn@NiFe-LDH before and after the durability test at a constant overpotential of 500 mV for 100 h.

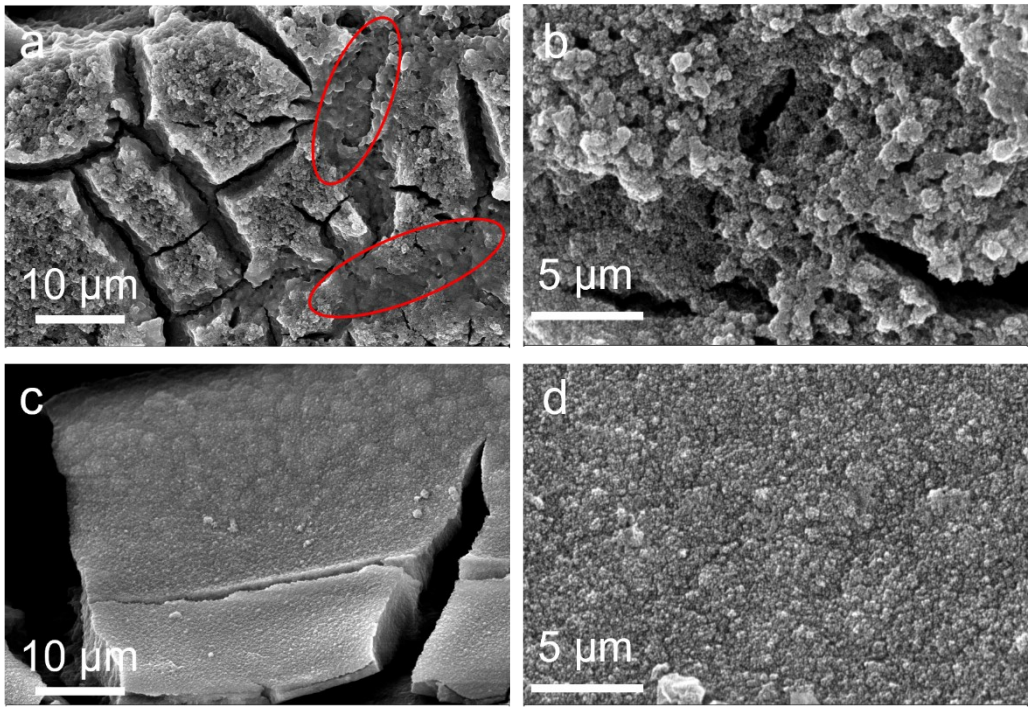

Fig. S12 SEM images of NiFe-LDH (a, b) and Zn@NiFe-LDH (c, d) after stability test.

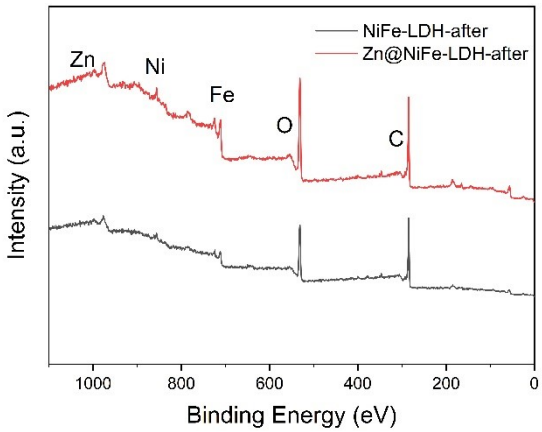

Fig. S13 XPS survey spectra of Zn-NiFe-LDH and Zn@NiFe-LDH after stability test.

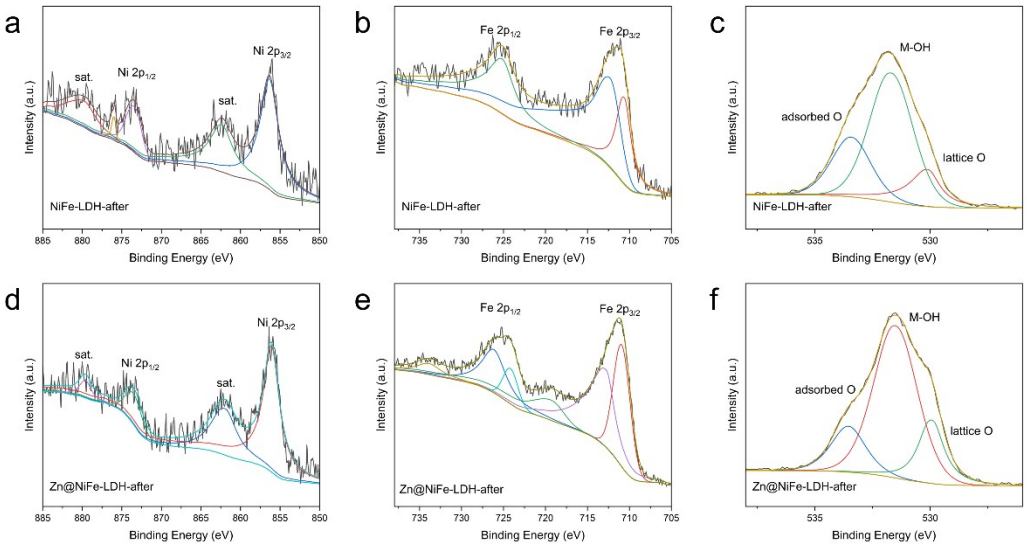

Fig. S14 High-resolution (a, d) Ni 2p spectra, (b, e) Fe 2p spectra, and (c, f) O 1s spectra for NiFe-LDH and Zn@NiFe-LDH after stability test.

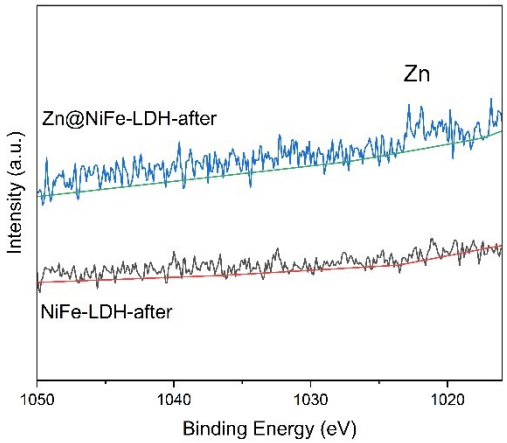

Fig. S15 High-resolution Zn 2p spectra of Zn-NiFe-LDH and Zn@NiFe-LDH after stability test.

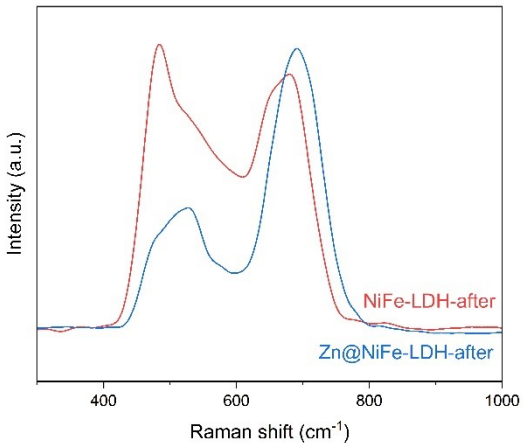

Fig. S16 Raman spectra of Zn-NiFe-LDH and Zn@NiFe-LDH after stability test.

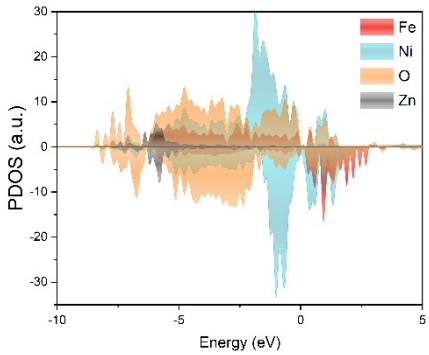

Fig. S17 The calculated DOS of metal 3d, oxygen 2p of surface Zn doped NiFe-LDH.

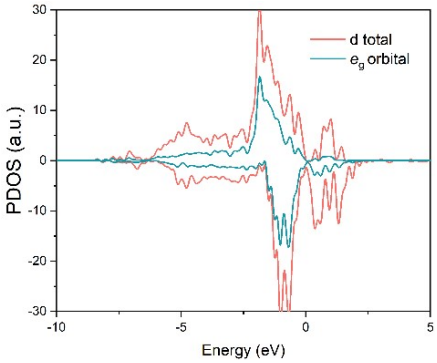

Fig. S18 Density of states projected onto Ni 3d orbitals and e_g orbitals of surface Zn doped NiFe-LDH.

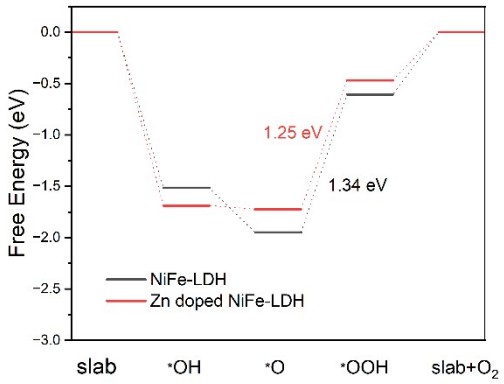

Fig. S19 The free energy change of the OER for NiFe-LDH and Zn doped NiFe-LDH.

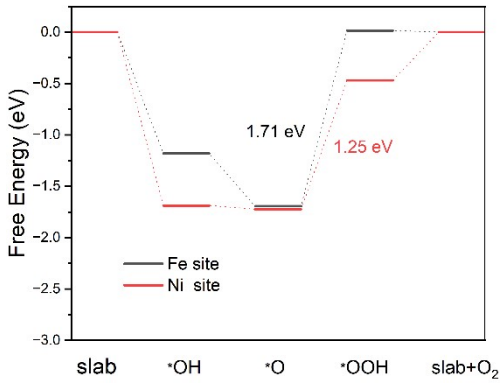

Fig. S20 The free energy change of the OER for Fe site and Ni site in Zn doped NiFe-LDH.

Table S1 Atomic ratio of different types of Ni bond from XPS deconvolution.

Sample	Ni^{2+}	Ni^{3+}
NiFe-LDH	100.00%	0.00%
Zn@NiFe-LDH	66.67%	33.33%
Zn-NiFe-LDH	81.30%	18.70%

Table S2 Atomic ratio of different types of Fe bond from XPS deconvolution.

Sample	Fe^{2+}	Fe^{3+}
NiFe-LDH	100.00%	0.00%
Zn@NiFe-LDH	81.30%	18.70%
Zn-NiFe-LDH	32.43%	67.57%

Table S3 The elements content results of different samlpes from XPS.

Sample	Fe (wt%)	Ni (wt%)	O (wt%)	Zn (wt%)
NiFe-LDH	3.87	4.32	48.95	/
Zn@NiFe-LDH	3.59	3.26	43.5	1.15
Zn-NiFe-LDH	5.47	1.89	43.2	2.21

Table S4 Atomic ratio of different types of O bond from XPS deconvolution.

Sample	M–O	M–OH	adsorbed O
NiFe-LDH	26.98%	52.91%	20.11%
Zn@NiFe-LDH	28.99%	34.78%	36.23%
Zn-NiFe-LDH	26.63%	50.25%	23.12%

Table S5 Comparison of OER performance of Zn@NiFe-LDH with other catalysts reported.

Catalysts	Overpotential at 10 mA/cm^{-2}	Overpotential at 100 mA/cm^{-2}	Stability	Tafel slope (mV dec^{-1})	Ref.
Zn@NiFe-LDH	216 mV at 10 mA/cm^{-2}	266 mV at 100 mA/cm^{-2} 326 mV at 300 mA/cm^{-2}	100 h at 1.73V	24.40	This work
NiFeLa	190 mV at 10 mA/cm^{-2}	248 mV at 100 mA/cm^{-2} 310 mV at 300 mA/cm^{-2}	600 h at 100 mA/cm^{-2}	34.4	Nano-Micro Lett. (2025) 17:11
NiFeZn-4	204 mV at 10 mA/cm^{-2}	/	10 h at 1.72V	64.6	Appl. Surf. Sci., 2023, 610, 155288
NiFeLDH-D1	241 mV at 10 mA/cm^{-2}	397 mV	48 h at 100 mA/cm^{-2}	54.9	*Langmuir* 2023, 39, 18152-18160
NiFeOOH-V_{Zn}	240 mV at 10 mA/cm^{-2}	/	120 h at 1.56V	19	*Small* **2024**, *20*, 2307069
NFN/NF-15h	208 mV at 10 mA/cm^{-2}	315 mV at 100 mA/cm^{-2}	/	113.9	*Langmuir* 2024, 40, 26339-26349
Ni_2Fe-LDH /$FeNi_2S4$	223 mV at 10 mA/cm^{-2}	240 mV at 100 mA/cm^{-2}	20 h at 50 mA/cm^{-2}	29.4	*Adv. Funct. Mater. 2022, 32, 2200951*
Ru/FeNiOOH@$NiPO_x$ /NF	172 mV at 10 mA/cm^{-2}	263 mV at 100 mA/cm^{-2}	100 h at 600 mA/cm^{-2}	32.4	*Adv. Funct. Mater.* ***2025****, 35, 2414493*
γ-FeOOH@$Ni(OH)_2$/NF	195 mV at 10 mA/cm^{-2}	213 mV at 100 mA/cm^{-2}	300 h at 100 mA/cm^{-2}	36.6	*ACS Sustainable Chem. Eng. 2024, 12, 6023-6034*
Fe-$Co(OH)_2$ /MoP	240 mV at 10 mA/cm^{-2}	344 mV at 100 mA/cm^{-2}	36 h at 120 mA/cm^{-2}	39.6	*Small* ***2025****,*

					e05953
SSF-F	230 mV at 10 mA/cm^{-2}	279 mV at 100 mA/cm^{-2}	550 h at 100 mA/cm^{-2}	44	*Int. J. Hydrog. Energy,* 2022, *45(3), 1810-1821*
ITE-EH301	264 mV at 10 mA/cm^{-2}	298 mV at 100 mA/cm^{-2} 311 mV at 300 mA/cm^{-2}	90 h at 800 mA/cm^{-2}	30.7	*Int. J. Hydrog. Energy,* 2025,*98(13), 985-994*
SSEAE	186 mV at 10 mA/cm^{-2}	289 mV at 100 mA/cm^{-2}	1600 h at 500 mA/cm^{-2}	31.4	*Adv. Funct. Mater. 2025, e16748*
NaOH/$NaIO_4$-SSF	207 mV at 10 mA/cm^{-2}	270 mV at 100 mA/cm^{-2}	100 h at 10 mA/cm^{-2}	42.5	*Chemistry Select 2025, 10,e03135*
NIO-SS	215 mV at 10 mA/cm^{-2}	391 mV at 100 mA/cm^{-2}	100 h at 10 mA/cm^{-2}	49.8	*J. Alloys Compd., 2023, 968 172097*
LaIr-Co_3O_4	236 mV at 10 mA/cm^{-2}	/	1000 h at 100 mA/cm^{-2}	70	*Nat. Commun. 2025, 16, 8145*
CuO_x/Co_3O_4	264 mV at 25 mA/cm^{-2}	308 mV at 100 mA/cm^{-2}	100 h at 100 mA/cm^{-2}	43.5	*ACS Nano 2025, 19, 21, 19938-19950*
Ru–Co_3O_4-TM-8h	243 mV at 10 mA/cm^{-2}	323 mV at 100 mA/cm^{-2}	100 h at 500 mA/cm^{-2}	65	*Int. J. Hydrog. Energy,* 2025,*106(6),528-536*
a-RNMO (Ru doped $NiMoO_x$)	220 mV at 10 mA/cm^{-2}	/	60 h at 100 mA/cm^{-2}	45.15	*Nat. Commun. 2025, 16, 8827*

Table S6 The electron occupancy of the e_g of Ni 3d orbital after Zn doping.

Sample	Occupancy (n)
NiFe-LDH	0.59
Body Zn doped	1.13
Surface Zn doped	0.75